Evaluating the effect of transmissive optic thermal lensing on laser beam quality with a Shack–Hartmann wave-front sensor

Justin D. Mansell, Joseph Hennawi, Eric K. Gustafson, Martin M. Fejer, Robert L. Byer, David Clubley, Sanichiro Yoshida, and David H. Reitze

We examine wave-front distortion caused by high-power lasers on transmissive optics using a Shack–Hartmann wave-front sensor. The coupling coefficient for a thermally aberrated Gaussian beam to the TEM_{00} mode of a cavity was determined as a function of magnitude of the thermally induced aberration. One wave of thermally induced phase aberration between the Gaussian intensity peak and the $1/e^2$ radius of the intensity profile reduces the power-coupling coefficient to the TEM_{00} mode of the cavity to 4.5% with no compensation. With optimal focus compensation the power coupling is increased to 79%. The theoretical shape of the thermally induced optical phase aberration is compared with measurements made in a neutral-density filter glass, Faraday glass, and lithium niobate. The agreement between the theoretical and the measured thermal aberration profiles is within the rms wave-front measurement sensitivity of the Shack–Hartmann wave-front sensor, which is a few nanometers.

OCIS codes: 120.5050, 120.3930, 140.3460, 140.6810.

1. Introduction

High-power lasers with excellent spectral- and spatial-mode properties are required for applications such as laser machining, medicine, quantum optics, nonlinear optics, fusion, and interferometry. Increasing laser power while maintaining laser beam quality requires careful consideration of beam distortion that can be caused by thermal and nonlinear optical effects. Thermal lensing in transmissive optics can be neglected for applications in which beam quality is not important. However, for applications such as the Laser Interferometric Gravitational-Wave Observatory (LIGO),[1] high beam quality at high power is critical.

The LIGO detector is a Michelson interferometer with 4-km-long arms, each containing a Fabry–Perot cavity designed to sense a phase change induced on a laser beam by a gravitational wave. Because the LIGO design specifies an M^2 of 1.1, any significant distortion of the beam reduces the beam quality below this specification. Although it is possible to compensate static aberrations with null-corrector plates, dynamic aberrations remain a problem for high-power lasers that require high beam quality. The dynamic aberrations we consider in this paper are caused by absorption of light that causes heating in the optical components and therefore an optical path-length change that distorts the beam. The first-generation LIGO receiver, called LIGO I, uses a 10-W Nd:YAG laser to illuminate the interferometer, so thermally induced aberrations are not severe enough to require active compensation. The first upgrade to LIGO, which is called LIGO II, may use a 180-W Nd:YAG laser, making the thermal distortions more than an order-of-magnitude worse and possibly necessitating some type of active compensation.

One possible technique to compensate for dynamic aberrations is an adaptive optics system.[2] Adaptive optics is an engineering technique developed by the astronomical community for sensing and compensating atmospheric aberrations that lead to reduced image quality. The typical adaptive optical system

J. D. Mansell (jmansell@Stanford.edu), J. Hennawi, E. K. Gustafson, M. M. Fejer, and R. L. Byer are with the Department of Applied Physics, Stanford University, 445 Via Palou Street, Stanford, California 94305-2130. D. Clubley is with the Department of Physics, University of Glasgow, Glasgow G128QQ, Scotland. S. Yoshida and D. H. Reitze are with the Department of Physics, University of Florida, Gainesville, Florida 32611.

Received 26 June 2000; revised manuscript received 25 September 2000.

0003-6935/01/030366-09$15.00/0

consists of a Shack–Hartmann wave-front sensor for determining the spatial phase of the wave front and a deformable mirror to compensate for the phase aberrations. Such systems typically operate at a closed-loop bandwidth of 100 Hz.[3] Although we would not consider active compensation of thermal distortions for many applications because of the increased cost and complexity, the combination of stringent spatial-mode specifications and the high laser power make active compensation a viable engineering solution for LIGO.

The Shack–Hartmann wave-front sensor used in modern adaptive optical systems is based on the original Hartmann test invented in 1900.[4] The Hartmann test, similar to interferometry, measures the spatial phase variation of a beam. In the Hartmann test, an opaque screen with an array of holes in it is placed in front of an optic under test. A known wave-front is then aberrated by the optic and passes through the Hartmann screen. The light is then allowed to propagate a known distance to an imaging device. The average wave-front tilt over each hole is determined based on the change in the transverse position of the diffracted spots on the screen. In 1971 Shack adapted the Hartmann technique for use in modern optical systems by replacing the opaque screen with an array of lenses. This allowed near-unity optical efficiency, which was important for astronomical applications. The resulting device is referred to as the Shack–Hartmann wave-front sensor.[3]

The technology developed for the Shack–Hartmann wave-front sensor has been commercialized for optical metrology[5] by use of CCD arrays, personal computers, and micro-optic lens arrays. The Shack–Hartmann wave-front sensor can be fabricated today for a fraction of the cost of interferometer systems and can achieve sensitivities comparable with those from commercial interferometers.[6] Moreover, the sensor typically operates at a measurement rate that is much faster than traditional interferometer systems and is vibration insensitive, thus eliminating the need for vibration isolation.

Here we evaluate thermal aberrations induced on laser beams by absorbing transmissive optics and evaluate the possibility of using the Shack–Hartmann wave-front sensor in an adaptive optical system to measure those aberrations. We begin by describing the shape of the thermal field in absorbing transmissive optics and how it affects the optical path length through the material. We show that the transmissive optic thermal aberration couples light from the lowest-order Hermite–Gaussian laser mode to higher-order modes. We then introduce and evaluate the Shack–Hartmann wave-front sensor as a tool for measuring the spatial profile of a thermal lens. Finally we conclude by commenting on the potential for the Shack–Hartmann wave-front sensor as a feedback element in an adaptive optical system for high-power lasers.

2. Thermally Induced Optical Path-Length Changes

Here we discuss the effect of absorption of a Gaussian laser beam by a transmissive optical component. We discuss the resultant thermal field distribution in the optic and calculate the effect on the optical path through the crystal. We give examples of some optical materials of interest to the LIGO project and evaluate how the induced optical path-length changes affect the laser beam quality.

A. Temperature Changes

Thermal lensing is caused by absorption in an optical medium and the subsequent optical path-length deformation caused by heating. The equation describing the temperature profile for a known heat source is given by[7]

$$\nabla^2 T + \frac{q}{k_{\mathrm{th}}} = \frac{1}{D_{\mathrm{th}}}\frac{\partial T}{\partial t}, \tag{1}$$

where T is the temperature, q is the heat source ($\mathrm{W/m^3}$), D_{th} is the thermal diffusivity, and k_{th} is the thermal conductivity (W/mK). Assuming that a Gaussian beam is transmitted through a sample with uniform absorption and that the heated sample is much larger than the heating beam and the heat flow is exclusively radial, Eq. (1) yields a steady-state temperature distribution given by[8]

$$\begin{aligned}\Delta T(r) &= |T(r) - T_0| \\ &= \frac{-aP}{4\pi k_{\mathrm{th}}}\left\{\Gamma + \ln\left[2\left(\frac{r}{w}\right)^2\right] + E_1\left[2\left(\frac{r}{w}\right)^2\right]\right\} \\ &= \frac{aP}{4\pi k_{\mathrm{th}}}\left[\sum_{n=0}^{\infty}\frac{(-1)^n\left(2\,\frac{r^2}{w^2}\right)^n}{nn!}\right],\end{aligned} \tag{2}$$

where a is the absorption coefficient per length, P is the incident power, Γ is Euler's constant (~ 0.577215), w is the TEM_{00} Gaussian beam radius, and E_i is the exponential integral function.[9] To compare different thermal fields quantitatively, here we define the magnitude of the thermal field as the temperature difference between the center of the Gaussian beam and the $1/e^2$ radius of the intensity profile, which is given by

$$\Delta T_{\mathrm{mag}} = |\Delta T(0) - \Delta T(w)| = 1.32\,\frac{aP}{4\pi k_{\mathrm{th}}} = 0.105\,\frac{aP}{k_{\mathrm{th}}}. \tag{3}$$

Often only the parabolic term of the series expansion is considered. This approximation, referred to as thermal lensing, makes the thermal distribution behave optically like a lens. However, the higher-order terms are important to consider because they can couple power from the TEM_{00} mode of a laser to higher-order modes and thus reduce the beam quality.

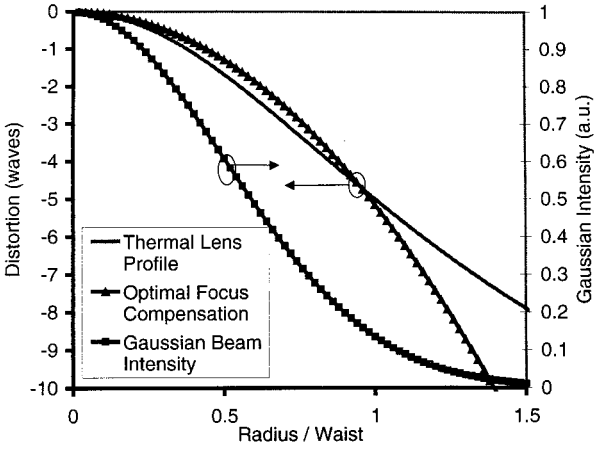

Fig. 1. Calculation of the transmissive optic thermal lens shape in waves assuming five waves of aberration between the center and the Gaussian waist with respect to distance from the center of the heating beam. The Gaussian intensity is also plotted to show how much power is in the beam with respect to the radius.

B. Thermally Induced Optical Path-Length Changes

Temperature changes in an optical medium result in optical path-length changes through a variety of mechanisms. The most prominent are the index-of-refraction changes that are due to temperature and strain and thermal expansion. These effects combine to produce an optical path length $\Lambda(r)$ through the optic given by

$$\Lambda(r) = n_0 L + [\Delta n_{\text{thermal}}(r)]L + [\Delta n_{\text{stress}}(r)] \times L + n_0[\Delta L_{\text{thermal}}(r)], \quad (4)$$

where n_0 is the material refractive index at a constant temperature, L is the length of the optic, $\Delta n_{\text{thermal}}(r)$ is the thermal shift in the refractive index, $\Delta n_{\text{stress}}(r)$ is the shift in the refractive index that is due to stress, and $\Delta L_{\text{thermal}}(r)$ is the shift in the length of the optic that is due to thermal expansion.

Figure 1 shows the optical path-length change of a Gaussian beam after it has been thermally distorted by transmission through an absorbing optic such that there are five waves of aberration between the center of the beam and the $1/e^2$ radius of the Gaussian intensity profile. The curve in Fig. 1 labeled optimal focus compensation is the parabolic curve that needs to be removed from the thermal lens to maximize the coupling of the thermally aberrated Gaussian beam with a planar wave-front Gaussian beam. The overlap integral calculation is introduced in Subsection 2.D, but we plotted the optimal parabolic wave-front distortion to illustrate the difference in shape between a parabola and the Gaussian beam thermal lens. Because parabolic wave-front compensation is effectively equivalent to changing the wave-front radius of curvature, we refer to it here as optimal focus correction. This type of correction can be achieved experimentally with a lens.

The component of an optical path-length change that is due to a refractive-index change can be written as

$$\Delta\Lambda_{\text{thermal}}(r) = \frac{dn}{dT} L \Delta T(r), \quad (5)$$

where dn/dT is the temperature-induced change in the refractive index, also called the thermo-optic coefficient.

The optical path-length change that is due to the photoelastic effect for isotropic materials such as glass or Faraday glass can be approximated by

$$\Delta\Lambda_{\text{stress}}(r) \approx -\frac{{n_0}^3}{2} \rho_{12} \alpha L \Delta T(r), \quad (6)$$

where ρ_{12} is the photoelastic coefficient and α is the thermal expansion coefficient. The photoelastic effect in crystals involves multiplication of the strain tensor by the photoelastic tensor to determine the refractive-index ellipsoid.[10] In Subsection 2.C we show that $\Delta\Lambda_{\text{stress}}(r)$ can be neglected for the optical materials considered here because the photoelastic effect is substantially smaller than the thermo-optic effect.

For thermal expansion of a long optic, the colder portion of the sample surrounding the heated portion exposed to the beam clamps the thermal expansion along the direction of propagation. Thus the thermal expansion can be neglected except at the ends of the sample. The region of the material at the ends of the sample that is not clamped by the colder region extends approximately a distance equal to a Gaussian beam-spot radius into the sample.[11] Therefore the optical path-length change that is due to a change in crystal length from thermal expansion can be approximated by

$$\Delta\Lambda_{\text{expansion}}(r) \approx 2\alpha n w \Delta T(r), \quad (7)$$

where α is the thermal expansion coefficient and w is the $1/e^2$ radius of the Gaussian intensity profile.

To discuss further the thermal lens in a quantitative fashion, here we define the thermal lens magnitude as the optical path-length change between the center of the beam and the $1/e^2$ radius of the Gaussian intensity profile. The thermal lens magnitude is thus given by

$$\Delta\Lambda_{\text{mag}} = |\Delta\Lambda(0) - \Delta\Lambda(w)|, \quad (8)$$

where w is again the $1/e^2$ radius of the Gaussian intensity profile.

Based on the analysis above, there are three major effects that can induce optical path-length changes by heating in absorptive optical materials that are used in transmitting laser beams. In the next section we show that, for materials of interest to the LIGO project, only the thermo-optic effect is important.

C. Thermal Lensing in Selected Optical Materials

Although many applications are affected by these thermal distortions, we evaluate thermal lensing effects specifically for LIGO. We elected to examine

Table 1. Optical and Thermal Parameters of Selected Optical Materials

Material	dn/dT (10^{-6} 1/K)	L (cm)	k_{th} (W/mK)	α (10^{-6}/K)	n_0	ρ_{12}	Absorption (%)
$LiNbO_3$ (extraordinary)	44	0.1	5.6	14.8	2.2	0.13 (ρ_{13})	35.7
FR5	7.5	5.0	0.84	4.7	1.7	0.26	5.0
Schott NG5 glass	5.1–6.3[a]	0.3	1.03	0.5	1.5	0.27	90
TGG	20	5.0	7.4	9.4	1.95	0.1[a]	1.0
Fused silica	10.1	10	1.38	0.5	1.5	0.270	0.0001[a]

[a]Estimate.

only materials that are used in transmission in delivering the LIGO laser to the interferometer. The mirrors and beam splitter that are used to form the interferometer are made of fused silica. Electro-optic modulators that are used to put sidebands on the laser beam for locking the length of the subsequent optical cavities are made of lithium niobate. The Faraday isolator made of Faraday glass (Tb_2O_3) or thallium gallium garnet (TGG) is used to isolate the laser from the optical system so that backreflections do not affect the laser performance. We measured the thermal distortions in lithium niobate, Hoya FR5 Faraday glass, and a sample of glass with high absorption, specifically an NG5 neutral-density (ND) filter. Table 1 shows the pertinent material properties of these samples, standard fused silica, and TGG, including dn/dT, length L, thermal conductivity k_{th}, thermal expansion α, the largest photoelastic coefficient ρ, and an independent measure of absorption for the measured samples.[12–15] High-absorption samples of lithium niobate and glass were chosen for our experiments to increase the thermal lensing induced by the relatively low-power 700-mW Nd:YAG laser that was available for our experiments.

Using Table 1, we calculated the thermally induced optical path-length change for the samples. Table 2 shows the thermo-optic, photoelastic, and thermal expansion calculated for a collimated 1-mm waist beam and a 5-cm-long sample.

For all the materials examined here, the optical path change that is due to thermal expansion yields a smaller contribution than the other two effects. In most of the materials, the refractive-index change with temperature is significantly larger than the stress-induced refractive-index change.

D. Modal Power Coupling

The effect of a nonspherical thermal lens on a Gaussian beam is to convert light from the TEM_{00} Gaussian mode into higher-order Hermite–Gaussian modes. The fraction of light coupled to the higher-order Hermite–Gaussian modes provides one way to evaluate laser beam quality. Kogelnik presented the theory of modal coupling coefficients in 1964.[16] He began by writing the electric field distribution of a two-dimensional Hermite–Gaussian laser mode, $TEM_{m,n}$, as the product of the electric fields of two one-dimensional Hermite–Gaussian modes, $\Psi_m(x)$ and $\Psi_n(y)$. Kogelnik showed that amplitude coupling in the x dimension, $c_x(\Psi_{\text{aberrated}}, \Psi_m)$, of an aberrated beam with an electric field $\Psi_{\text{aberrated}}(x)$ to a one-dimensional Hermite–Gaussian mode, $\Psi_m(x)$, is determined by the overlap integral

$$c_x(\Psi_{\text{aberrated}}, \Psi_m) = \int_{-\infty}^{+\infty} \Psi_m(x)\Psi_{\text{aberrated}}^*(x)\mathrm{d}x. \quad (9)$$

The same relationship holds for the y dimension. The two-dimensional amplitude coupling coefficient between electric field is then the product of the two orthogonal one-dimensional coupling coefficients, or $c_x(\Psi_{\text{aberrated}}, \Psi_m)\ c_y(\Psi_{\text{aberrated}}, \Psi_n)$. Furthermore, Kogelnik showed that the power coupled from an incoming beam to an outgoing TEM_{00} mode beam κ is the product of the two-dimensional electric field coupling coefficient to the TEM_{00} Hermite–Gaussian mode and its complex conjugate, or

$$\begin{aligned}\kappa &= [c_x(\Psi_{\text{aberrated}}, \Psi_m)c_x^*(\Psi_{\text{aberrated}}, \Psi_m)] \\ &\quad \times [c_y(\Psi_{\text{aberrated}}, \Psi_n)c_y^*(\Psi_{\text{aberrated}}, \Psi_n)] \\ &= \kappa_x\kappa_y. \end{aligned} \quad (10)$$

This problem has been addressed in the literature under the assumption that the thermal aberration is small.[8] As the laser beam power increases, this approximation no longer holds.

By evaluating the overlap integral numerically, we

Table 2. Calculated Optical Path-Length Changes

Material	$\Delta\Lambda_{\text{thermal}}/\Delta T(r)$ (μm/K)	$\Delta\Lambda_{\text{stress}}/\Delta T(r)$ (μm/K)	$\Delta\Lambda_{\text{expansion}}/\Delta T(r)$ (μm/K)
$LiNbO_3$	2.2	−0.51	0.065
Hoya FR5	0.38	−0.15	0.016
Schott NG5	0.29	−0.011	0.0015
TGG	1.0	−0.17	0.0367
Fused silica	0.5	−0.011	0.0015

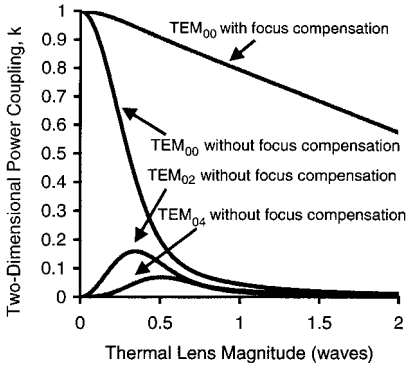

Fig. 2. Two-dimensional power coupling κ between a Gaussian beam with a thermal lens and an ideal TEM_{00} beam with and without optimal focus compensation. The power coupling of the aberrated beam with optimal focus compensation to the TEM_{20} Hermite–Gaussian mode is also shown.

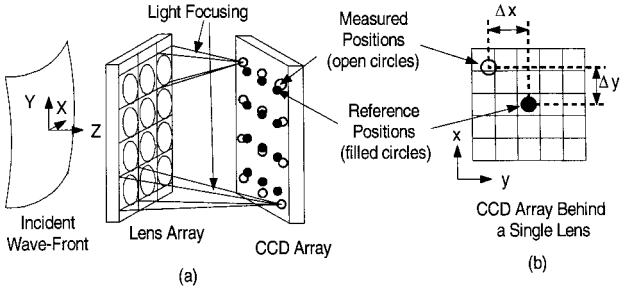

Fig. 3. Schematic of the operation of the Shack–Hartmann wave-front sensor. (a) Light incident on the sensor propagates along the z axis. The CCD array and the lens array are shown tilted relative to each other only to illustrate the operation of the device. In reality, the lens array and the CCD array are parallel. (b) Schematic of the measured position change of the focal spots where Δx and Δy give the average wave-front tilt over a lens aperture when divided by the separation between the lens array and the CCD.

calculated the magnitude of the coupling between a planar wave-front Gaussian beam aberrated with a thermal lens and an ideal planar wave-front Gaussian beam. Both the thermally aberrated beam and the Hermite–Gaussian beams were normalized so that the maximum magnitude of the coupling coefficient is unity. Figure 2 shows the power coupling between a Gaussian beam with a planar wave front and a Gaussian beam with a thermal lens versus thermal lens magnitude. Assuming that the thermo-optic effect dominates, the thermal lens magnitude is given by

$$\Delta\Lambda_{\mathrm{mag}} = |\Delta\Lambda(0) - \Delta\Lambda(w)| = 1.32\,\frac{P_{\mathrm{abs}}}{4\pi k_{\mathrm{th}}}\frac{\mathrm{d}n}{\mathrm{d}T} = 0.105\,\frac{P_{\mathrm{abs}}}{k_{\mathrm{th}}}\frac{\mathrm{d}n}{\mathrm{d}T}, \quad (11)$$

where P_{abs} is the amount of absorbed power. One wave of thermal lens magnitude reduces the power coupling to a planar wave-front TEM_{00} laser beam to only 4.5%. Applying optimal focus correction increases the power-coupling coefficient to 79%. One wave of distortion at a wavelength of 1064 nm in a piece of 10-cm-thick 20-parts per million/cm absorption fused silica similar to that used in the LIGO I design is reached at 160 kW of laser power, independent of the beam diameter.

If the laser is impedance matched properly to a high-finesse cavity with a large high-order-mode axial mode separation, and therefore little intermode coupling, the power-coupling coefficient is the fraction of laser power that is coupled into the cavity. The overlap integral calculation shown in Fig. 2 allows an optical designer to formulate a thermal lens budget and determine an upper limit on the laser power allowed to transmit through the conditioning optics before the interferometer for a given acceptable amount of coupling loss. If the thermally induced distortions were compensated by an adaptive optical system before the interferometer, the power transmitted through the conditioning optics could increase. In Section 3, we evaluate the Shack–Hartmann wave-front sensor as a possible feedback sensor in such an adaptive optical system that allows active compensation of thermally induced beam distortion.

3. Shack–Hartmann Wave-Front Sensor

We used the Shack–Hartmann wave-front sensor to measure the changes in the optical path length in our experimental evaluation of thermal lensing. The changes in the optical path-length directly affected the measured wave front, which is defined as a surface of uniform phase that is normal to the propagation direction. Therefore a uniform plane wave has a planar wave front. In the case of thermal lensing of transmissive optics, the wave-front shape is given by Eqs. (2) and (4) and is illustrated in Fig. 1.

The modern Shack–Hartmann wave-front sensor consists of an array of lenses mounted in front of a charge-coupled device (CCD). Figure 3 shows a schematic of the operation of the wave-front sensor. Light travels to the sensor along the z axis. The CCD lies at the focal plane of the lens array. Each of the lenses acts like an optical lever, displacing the focal spot proportional to the average phase tilt over the lens. We used the wave-front sensor to measure the tilt over each lens by comparing the measured positions of the focal spots with the positions of the focal spots for a reference input beam. We then converted the tilt measurements into a replica of the wave front by performing a form of integration called wave-front reconstruction. For our measurements we chose a commercially available Shack–Hartmann wave-front sensor comprised of a lens array with 144-μm-diameter square lenses and an 8-mm focal length and a CCD with 10-μm pixels.[5]

The coordinate system shown in Fig. 3 illustrates the operation of the wave-front sensor. The z axis is the optical axis and is normal to the plane of the CCD and the lens array. The x and y axes are located in the plane of the CCD array. We calibrated the sensor by recording an image of a uniform plane wave.

We then determined the focal spot locations from this image by calculating their centroids or first moments along both the x axis and the y axis. The centroid in the x direction, x_{position}, of a single intensity pattern is defined by

$$x_{\text{position}} = \frac{\int_{-\infty}^{\infty}\int_{-\infty}^{\infty} I(x, y)x\mathrm{d}x\mathrm{d}y}{\int_{-\infty}^{\infty}\int_{-\infty}^{\infty} I(x, y)\mathrm{d}x\mathrm{d}y}, \tag{12}$$

where $I(x, y)$ is the intensity as a function of x and y, x is the location at which the intensity is measured along the x axis, and y is the location at which the intensity is measured along the y axis. Equation (12) needs to be modified to apply it to the Shack–Hartmann wave-front sensor. The CCD behind the Shack–Hartmann wave-front sensor is comprised of a set of discrete pixels that we describe by the variable i along the x axis and j along the y axis. This allows us to replace the integral with a summation. Furthermore, we have to change the limits of the integration to apply this formula to measuring an array of focal spots. We assume that the intensity pattern at the focus of a given lens can be bounded effectively by the edges of the lens. We typically use square lenses in building Shack–Hartmann wave-front sensors with diameters equal to an integer number of pixels, which makes the mapping of the lens boundaries onto the rectangular array of pixels of the CCD straightforward. Using index coordinates, we call the pixel corresponding to the lower left corner of the lens $(i_{\min}, j_{\min})$ and the pixel corresponding to the upper right corner of the lens $(i_{\max}, j_{\max})$. Therefore Eq. (12) can be rewritten as

$$x_{\text{position}} = \frac{\sum_{i=i_{\min}}^{i_{\max}}\sum_{j=j_{\min}}^{j_{\max}} I(i, j)i}{\sum_{i=i_{\min}}^{i_{\max}}\sum_{j=j_{\min}}^{j_{\max}} I(i, j)} s_x, \tag{13}$$

where $I(i, j)$ is the intensity measured by the pixel in the ith row and the jth column and s_x is the spacing of pixels along the x axis. Eq. (13) can be used to determine the position of the focal spot along the y axis.

A wave-front measurement can be made after the reference focal spot locations have been determined. The Shack–Hartmann wave-front sensor is illuminated with a beam whose wave front $\Phi(x, y)$ is being measured, and the focal spot positions are determined from the CCD image by use of Eq. (13). For this discussion we limit ourselves to considering the x axis, but the y axis can be treated in the same fashion. Also we assume that the CCD has been placed at the exact focal plane of the lens array. The change in focal spot position along the x axis, Δx, is obtained when we subtract the measured focal spot positions. The measured two-dimensional wave-front is designated by the variable $\phi(x, y)$. The average gradient of the wave front over the lens diameter along the x axis is calculated with

$$\frac{\mathrm{d}\phi(x, y)}{\mathrm{d}x} = \frac{\Delta x}{f}, \tag{14}$$

where f is the lens focal length.

Once the local wave-front slopes have been determined, we can reconstruct the wave front by performing a type of integration on the gradient measurements. The two types of wave-front reconstruction algorithm are zonal and modal.[17] The zonal wave-front reconstruction is a type of numerical integration. The modal wave-front reconstruction fits the data to a set of orthogonal modes. In this paper a zonal reconstructor is used to generate the wave fronts from the measured wave-front gradients. The zonal reconstructor generates two wave fronts by integrating the measured slopes along the x and the y directions. The resulting wave front is the sum of the integration in both directions.

It is important to understand the sensitivity limitations of the wave-front sensor for measuring weak transmissive optic thermal lenses. The sensitivity of the wave-front sensor depends on the sensor's ability to determine the position of the focal spots on the CCD array. The error in determining the focal spot location includes a set of factors such as CCD detector noise, coherent optical cross talk between lenses, and CCD digitization error. We measured the rms error in the focal spot location for the wave-front sensor by evaluating the spot position of a stable wave front repeatedly with the sensor and by calculating the average and rms error in this determination. The rms error in focal spot location, Δx_{rms}, for our wave-front sensor was approximately 0.1 μm for a planar wave front. It is possible to have errors in the measurement of the focal spot locations that are larger because of a variety of factors including coherent optical cross talk between adjacent array detector elements.

We measured the rms wave-front error by illuminating the sensor with a beam of uniform intensity with a planar wave front. The sensor evaluates the wave front many times and determines the rms difference between the individual measured wave fronts and an average wave front evaluated at each of the lenses. The rms wave-front error ϕ_{rms} of a Shack–Hartmann wave-front sensor is related to the quality of the reconstruction algorithm, the focal length of the lenses, the diameter of the lenses, and the rms spot location error. The ϕ_{rms} can be written as

$$\phi_{\text{rms}} \approx F_{\text{reconstructor}} \frac{d}{f} \Delta x_{\text{rms}}, \tag{15}$$

where $F_{\text{reconstructor}}$ is a factor determined empirically by the type of reconstructor used, d is the diameter of a lens in the lens array, and f is the lens focal length. Usually the rms error in spot position is the same along the x axis and along the y axis, but if it is not then the rms wave-front error in the two orthogonal

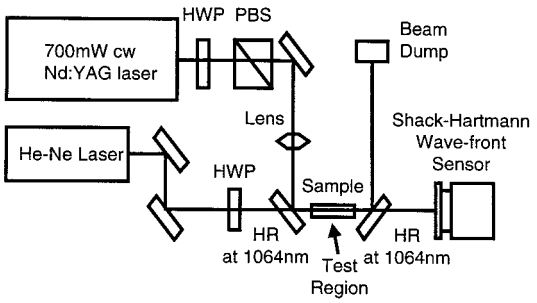

Fig. 4. Diagram showing the setup used to measure thermal lensing. Light from the 700-mW Nd:YAG laser travels through a half-wave plate (HWP) and a polarizing beam splitter (PBS) to control the laser power in the test region. The lens adjusts the Nd:YAG beam size in the test region. The high-reflector mirrors (HR) at 1064 nm are used to bring the Nd:YAG laser into and out of the test region. The He–Ne beam passes through a HWP to control polarization and is aligned collinear with the Nd:YAG beam in the test region through the dielectric HR mirrors. The Shack–Hartmann wave-front sensor measures the spatial phase of the He–Ne laser.

directions will differ. We measured the value of the reconstructor factor for the zonal reconstructor that we used to be approximately three, so the rms wave-front error was approximately 5 nm or approximately $\lambda/100$ for 633-nm light over the entire wave-front sensor aperture.

The Shack–Hartmann wave-front sensor can be used to make differential wave-front measurements in addition to making measurements with an optical flat as a reference. The sensor is set up in an optical system, and an image is recorded by the CCD array to form a new reference file. By comparing a measured result to the reference file, we measured only changes to the wave-front. This technique allows any aberrations in the optical system to be nulled such that only the newly induced optical path-length change is measured. The Shack–Hartmann wave-front sensor was used in this differential mode to measure thermal lensing.

4. Measurements

Active wave-front correction can only compensate for distortions if the feedback sensor can determine the distortions accurately. We propose to use a Shack–Hartmann wave-front sensor to make these measurements. In this section we demonstrate experimentally the capability to make measurements of thermally induced optical distortion in some materials of interest to the LIGO project using the Shack–Hartmann wave-front sensor. We also verify the effect of a thermal distortion on the laser beam by coupling a thermally aberrated beam into a Fabry–Perot ring cavity.

A. Thermal Lens Profile Measurements

Figure 4 shows a schematic of the experimental setup that we used for evaluating thermal lensing. A probe 1-mW He–Ne laser beam was aligned collinearly with a 700-mW Nd:YAG heating laser. The He–Ne laser was used as a probe laser to take advantage of the increased CCD array sensitivity at 633 nm. In addition, coherent optical cross talk between the focal spots on the CCD array was less at 633 nm than at 1064 nm, so the sensor was more accurate. The 1064-nm laser was used as the pump laser to simulate the effects of the high-power Nd:YAG laser that will be used in the LIGO project. The Nd:YAG laser power incident on the sample was controlled with a half-wave plate and polarizing beam splitter. A high reflector at 1064 nm was used to combine and separate the two lasers before and after the interaction region. After the system was aligned, a reference frame was taken with the Nd:YAG laser blocked and the sample cool. Then the Nd:YAG laser was transmitted through the sample, and we measured the induced thermal lens by comparing it with the reference image. With this differential technique, the static aberrations in the optical system were removed from the measurement.

The thermal lens was measured with the Shack–Hartmann wave-front sensor, and the shape was compared with that predicted by Eqs. (2) and (4). Some simplifications were made in the analysis. As Table 2 shows for the materials we studied, the change in the refractive index with temperature is the largest term in the optical path-length change for long crystals. Because the other effects that change the refractive index were small, they were neglected in the measurements except for the FR5 measurements for which the photoelastic effect was included. We reduced the two-dimensional wave front to a radial plot by identifying the center of the wave front and by averaging along equal radius lines. In this way the measurement and the theory could be compared directly because Eq. (2) gives a radial profile. Furthermore, this technique allows us to average along a given radius and thereby reduce the rms wave-front error from the 5 nm measured in two dimensions.

Figure 5 shows the measured thermal lens for 190 mW of Nd:YAG power with a 1.02-mm waist beam incident on a 3-mm-thick piece of NG5 filter glass. Low-absorption fused silica used by LIGO produces too little thermal distortion with a 700-mW Nd:YAG pump beam to be seen by our Shack–Hartmann wave-front sensor, so Schott glass NG5 ND filter was used instead. The ND filter exhibited the largest thermal aberration because of its high absorption. The filter exhibited the theoretical thermal lensing shape with 1.5-nm rms error to the fit and 105 nm of thermal lens magnitude. The absorption of this filter was provided by the manufacturer and measured independently, but the thermo-optic coefficient was estimated by the manufacturer to lie between 5.1×10^{-6} and 6.3×10^{-6}/°C. The best fit to the data was used to extract a measured thermo-optic coefficient of 5.8×10^{-6}/°C.

A 5-cm-long and 1-cm-diameter piece of FR5 Faraday glass manufactured by Hoya was investigated. The absorption of this material is far less

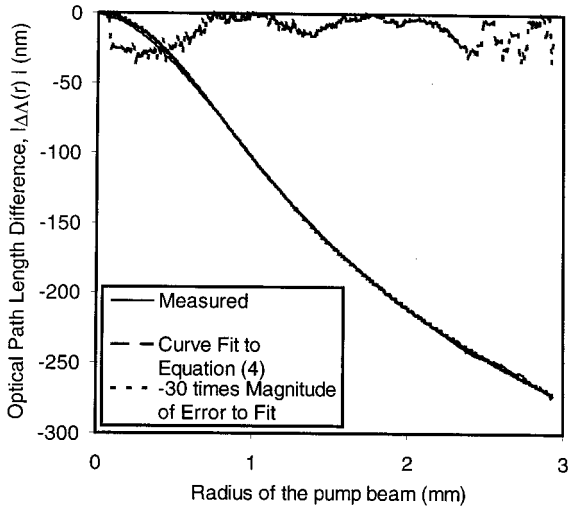

Fig. 5. Optical path-length difference versus the radius of the pump beam for NG5 Schott glass when exposed to a 190-mW Nd:YAG beam with a Gaussian waist of 1.02 mm. Shown is the measured data, the fit to the theoretical shape given by Eq. (2), and the absolute value of the difference between the two curves expanded 30 times to make the difference visible.

than that of the absorbing glass, and thus even with higher laser power the measurement error was increased. The total optical path-length change between the center of the beam and a distance three times the radius of the intensity profile was only 58 nm. By fitting the profile measured with 680 mW of cw Nd:YAG laser power in a 340-μm radius beam to Eq. (2), we extracted an absorption of 5.9% using the thermo-optic and photoelastic refractive-index effects. This differs from the independent absorption measurement by 0.9%. The rms error to the fit was 1.85 nm. The error in this extraction of the absorption is due to the small thermal lens magnitude.

Thermal lensing in a wafer of lithium niobate was also evaluated. We used a special high-absorption sample of lithium niobate in our experiments because the high-grade lithium niobate used in LIGO has too little absorption for it to be detectable with the 700-mW pump laser (the specification is less than 10^{-3} cm^{-1} at 1064 nm). The lithium niobate sample was treated in a high-temperature oven in an oxygen-depleted environment to increase its absorption. The absorption was measured externally to be 37% through the entire 1-mm-thick sample. We tested the sample by the wave-front sensor using a collimated 1-mm waist pump beam. The thermal profile had a total phase deviation between the center of the beam and the point three times the $1/e^2$ radius of the intensity profile from the center of 207 nm with a rms error of 6.9 nm to the fit. Absorption of 36.2% was extracted from the fit. The large rms error to the fit in this case is due to the power being absorbed in a short distance relative to the beam diameter, thus changing the thermal boundary conditions from a long cylinder to a short disk.

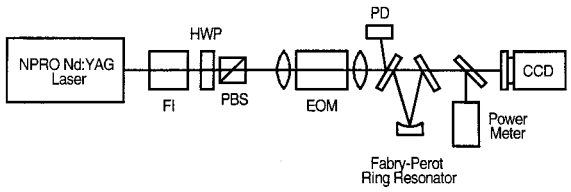

Fig. 6. Schematic of the optical setup used to measure the effect of transmissive optic thermal lensing on coupling to the TEM_{00} mode of a cavity. Note that the wave-front conditioning optics are not shown. An absorbing piece of filter glass, also not shown, was placed at different locations relative to the cavity waist. HWP, half-wave plate; PD, photodiode; NPRO, nonplanar ring-oscillator; FI, Faraday isolator; PBS, polarizing beam splitter; EOM, electro-optic modulator.

B. Effect of Thermal Lens on Beam Quality

Before reaching the interferometer, the LIGO optical system couples a high-power Nd:YAG laser into a series of Fabry–Perot ring cavities to filter the spatial and temporal noise of the laser.[18] These ring resonators are often referred to as mode cleaners because when they are aligned properly and locked to the laser, they reflect the laser light not coupled into the TEM_{00} mode of the cavity and transmit only TEM_{00} mode laser light. To verify our overlap integral calculations above, we induced a thermal lens on a Gaussian beam and used a mode cleaner as a filter to separate the TEM_{00} mode from the rest of the beam.

Figure 6 shows the experimental setup. A 700-mW nonplanar ring oscillator laser is transmitted through a Faraday isolator to avoid backreflections into the laser. The laser beam then illuminates a half-wave plate and a polarizing beam splitter to control the optical power through the rest of the optical system. An electro-optic modulator (EOM) induces frequency sidebands on the laser for radio-frequency cavity locking. The beam size, radius of curvature, direction, and position are then matched to the cavity through a series of lenses and mirrors, which for simplicity are not shown in Fig. 6. A photodiode is used to monitor light that reflects from the cavity. The ring mode cleaner that we used has a finesse of 4100, a round-trip length of 42 cm, and a Gaussian waist of 371 μm. Light that transmits through the cavity is split such that 70% illuminates a powermeter and 30% illuminates a CCD array used to monitor the cavity mode. During the experiment, ND filters were placed at different locations in the optical beam to attenuate the laser power and create a thermal lens.

We measured the power transmitted through the mode-cleaner cavity while varying the input power by rotating the half-wave plate. Figure 7 shows the measured power coupling with respect to the induced thermal lens magnitude. The thermal lens magnitude was calculated based on Eq. (11). Data taken with small induced thermal lens magnitudes have a large variation, but at higher thermal lens magnitudes the theory and experimental measurements agree well. This experiment shows that an uncom-

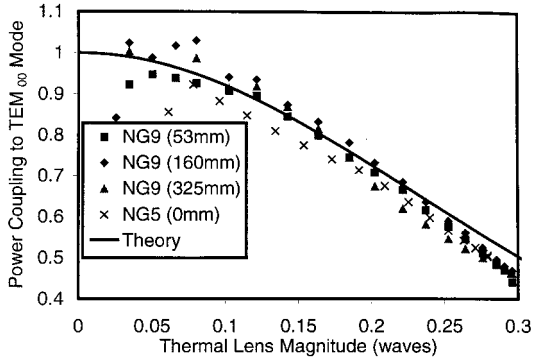

Fig. 7. Power coupling of a thermally distorted TEM_{00} mode to a ring Fabry–Perot mode-cleaner cavity versus the thermal lens magnitude induced in different types of filter glass (NG9 and NG5) at different distances from the cavity waist. For the measurement with the NG5, the thermal lens was reimaged into the cavity to eliminate any change in the Gaussian beam intensity profile. The thermal lens magnitude was calculated with the known material parameters and Eq. (11).

pensated thermal lens leads to a significant decoupling of the laser energy from the mode-cleaner Fabry–Perot cavity and thus limits the incident intensity.

5. Implications for LIGO II

In the LIGO II design, a TGG Faraday isolator and a lithium niobate EOM will be placed between the laser and the first mode cleaner. Commercial TGG has an absorption of 0.2%/cm at 1064 nm, and a length of approximately 5 cm is required for the Faraday isolator. Commercial lithium niobate absorption is approximately 0.1%/cm, and approximately 5 cm will be required for the EOM. With these absorption levels and lengths, a 180-W Nd:YAG laser beam will induce a thermal lens with a thermal lens magnitude of 30 nm in the lithium niobate and 22 nm in the TGG for a total distortion of 52 nm, which is approximately $\lambda/20$ at 1064 nm. This level of distortion is above the largest rms wave-front error measured by the Shack–Hartmann wave-front sensor by a factor of 7.5, thus making the wave-front sensor quite capable of seeing the distortions, which may be important for later adaptive optics compensation. Figure 2 shows that the effect of a $\lambda/20$ thermally induced distortion is to reduce the power in the TEM_{00} mode by 2.0% without any compensation or by 0.16% with parabolic wave-front compensation.

6. Conclusions

We have used a Shack–Hartmann wave-front sensor to measure thermally induced wave-front distortion in transmissive optics. We calculated that one wave of thermal lens magnitude results in a reduction of the power-coupling coefficient to the TEM_{00} Gaussian mode to 4.5%. Optimal focus correction of this beam can increase the power-coupling coefficient to 79%. We calculated that a thermal lens will be formed in the LIGO II Faraday isolator and EOM with a magnitude of 52 nm. We conclude that the Shack–Hartmann wave-front sensor has sufficient sensitivity to measure thermal aberrations in the LIGO II signal conditioning optics and therefore could be used in an adaptive optical system for control of wave-front distortion.

References and Notes

1. A. Abramovici, W. E. Althouse, R. W. P. Drever, Y. Gursel, S. Kawamura, F. J. Raab, D. Shoemaker, L. Sievers, R. E. Spero, K. S. Thorne, R. E. Vogt, R. Weiss, S. E. Whitcomb, and M. E. Zucker, "LIGO: the Laser Interferometer Gravitational-Wave Observatory," Science **256,** 325–333 (1992).
2. R. Q. Fugate, B. L. Ellerbroek, C. H. Higgins, M. P. Jelonek, W. J. Lange, A. C. Slavin, W. J. Wild, D. M. Winker, J. M. Wynia, J. M. Spinhirne, B. R. Boeke, R. E. Ruane, J. F. Moroney, M. D. Oliker, D. W. Swindle, and R. A. Cleis, "Two generations of laser-guide-star adaptive-optics experiments at the Starfire Optical Range," J. Opt. Soc. Am. A **11,** 310–324 (1994).
3. R. Tyson, *Principles of Adaptive Optics*, 2nd ed. (Academic, New York, 1998).
4. J. Hartmann, "Bemerkungen uber den Bau und die Justirung von Spektrographen," Z. Instrumentenkd. **20,** 47 (1900).
5. The cubic spline reconstructor is provided in the CLAS-2D software by WaveFront Sciences, Inc., Albuquerque, N.M. 87123.
6. D. R. Neal, D. J. Armstrong, and W. T. Turner, "Wave-front sensors for control and process monitoring in optics manufacture," in *Lasers as Tools for Manufacturing II*, L. R. Migliore and R. D. Schaeffer, eds., Proc. SPIE **2993,** 1–10 (1997).
7. W. M. Rohsenow, J. P. Hartnett, and E. N. Ganic, eds., *Handbook of Heat Transfer Fundamentals*, 2nd ed. (McGraw-Hill, New York, 1985), Chap. 4.
8. K. A. Strain, K. Danzmann, J. Mizuno, P. G. Nelson, A. Rudiger, R. Schilling, and W. Winkler, "Thermal lensing in recycling interferometric gravitational wave detectors," Phys. Lett. A **194,** 124–132 (1994).
9. M. Abramowitz and I. Stegun, eds., *Handbook of Mathematical Functions* (Dover, New York, 1965), pp. 227–231.
10. A. Yariv and P. Yeh, *Optical Waves in Crystals* (Wiley, New York, 1984), pp. 318–323.
11. A. Alexandrovski, Research Associate, Stanford University, Stanford, Calif. (personal communication, 1998).
12. M. M. Fejer and P. F. Bordiu, "Inorganic crystals for nonlinear optical frequency conversion," Annu. Rev. Mater. Sci. **23,** 321–379 (1993).
13. J. Storms, Hoya Corporation, 101 Metro Dr., Suite 500, San Jose, Calif. 95110 (personal communication, 1998).
14. B. Scheller, Schott Glass Technologies Inc., 400 York Ave., Duryea, Pa. 18642-2026 (personal communication, 1998).
15. R. Waynant and E. Marwood, *Electro-optics Handbook* (McGraw-Hill, New York, 1994), pp. 11.13–11.83.
16. H. Kogelnik, "Coupling and conversion coefficients for optical modes," in *Symposium on Qusi-Optics* (Polytechnic Institute of Brooklyn, Brooklyn, N.Y., 1964), pp. 333–347.
17. W. H. Southwell, "Wave-front estimation from wave-front slope measurements," J. Opt. Soc. Am. **70,** 998–1006 (1980).
18. N. Uehara, E. K. Gustafson, M. M. Fejer, and R. L. Byer, "Modeling of efficient mode matching and thermal-lensing effect on a laser-beam coupling into a mode-cleaner cavity," in *Modeling and Simulation of Higher-Power Laser Systems IV*, U. O. Farrukh and S. Basu, eds., Proc. SPIE **2989,** 57–68 (1997).